

Properties of the new divertor IIb in ASDEX Upgrade

R. Neu, J.C. Fuchs, G. Haas, A. Herrmann, A. Kallenbach, M. Laux, J. Neuhauser, F. Ryter, J. Gafert, O. Gruber, M. Kaufmann, B. Kurzan, V. Mertens, H.W. Müller, V. Rohde, A. Sips, J. Stober, B. Streibl, W. Treuterer and the ASDEX Upgrade Team

Max-Planck-Institut für Plasmaphysik, EURATOM-Association, Boltzmannstr.2, D-85748 Garching, Germany

Abstract.

A new divertor configuration (DIV IIb) is implemented in ASDEX Upgrade. In order to accommodate a large variety of plasma shapes with bottom triangularities (δ_{bot}) up to 0.48, the outer strike point region was modified and the roof baffle was lowered and diminished at its outer part. The inner part of the divertor strike point module remained unchanged, but at the divertor entrance a smooth transition to the inner heat shield is provided to minimize local hydrogen recycling. According to experiences with power handling in DIV II, ordinary fine grain graphite has been chosen for the outer strike point and the tiles are slightly tilted in toroidal direction to hide the leading edges. A first characterization of DIV IIb reveals, that the beneficial behaviour of DIV II is essentially maintained. There is an increase of the power density due to geometrical reasons at the outer target whereas the divertor radiation for similar magnetic configurations is almost unchanged. The good pumping characteristics for D and He are almost retained, suggesting a large influence of the inner divertor leg, the configuration of which remained unchanged. A significant reduction (20%) of the L-H threshold is observed pointing to lower densities upstream in the midplane as indicated by Li-beam measurements.

PACS numbers: 52.55.Rk, 52.40.Hf, 52.55.Fa

1. Introduction

In 1997 the original "open" ASDEX Upgrade Divertor I (DIV I) was replaced by the rather "closed" LYRA-Divertor (DIV II) [1]. In support of ITER, this DIV II (Fig. 1, left part) had been designed for optimal divertor radiation volume losses, high pumping efficiency etc, if used in connection with a narrow class of well-fitting low δ equilibria. These expectations were, in fact, nicely confirmed during a several years run period [1, 2]. In parallel to these optimized divertor studies, there was increasing interest in strongly shaped, especially higher triangularity plasmas, because of their improved confinement at high plasma density, the possible access to type-II Elms etc. [3, 4, 5, 6]. Since the top and bottom triangularities are coupled in ASDEX Upgrade due to operational reasons, these plasmas could only be produced in the DIV II geometry by positioning the outer divertor plasma leg on the top of the roof baffle located between the two curved vertical targets. Therefore some of the DIV II benefits were degraded, especially the power load characteristics and the pumping capability of the cryo-pump placed in the outer divertor region. To overcome this, the roof baffle and the outer part of DIV II were redesigned (DIV IIb) to accommodate a large variety of plasma shapes with high triangularities (δ_{bot}) up to 0.48 (Fig.1, right part: $\delta_{bot} = 0.48$), with the best strike point fitting to the pumping gaps obtained for medium δ equilibria.

2. Setup of Divertor IIb and Diagnostics

According to the positive experience with power handling in DIV II, ordinary fine grain graphite has been chosen for the outer strike point region in DIV IIb [7]. The tiles are slightly tilted in toroidal direction (as they were in DIV II) in order to hide the leading edges. In the poloidal cross section (Fig.1, right part), the outer strike-point module forms a straight line with larger poloidal angle to the flux surfaces than in DIV II. The resulting incidence angle of magnetic field lines has therefore increased from values below 2° to values around 4° . The inner part of the divertor

strike point module remained unchanged, but at the divertor entrance a smooth transition to the inner heat shield is provided to minimize local hydrogen recycling there. The roof baffle is lowered and diminished at its outer part to allow the outer divertor plasma leg to hit the strike point module even for the highest triangularities.

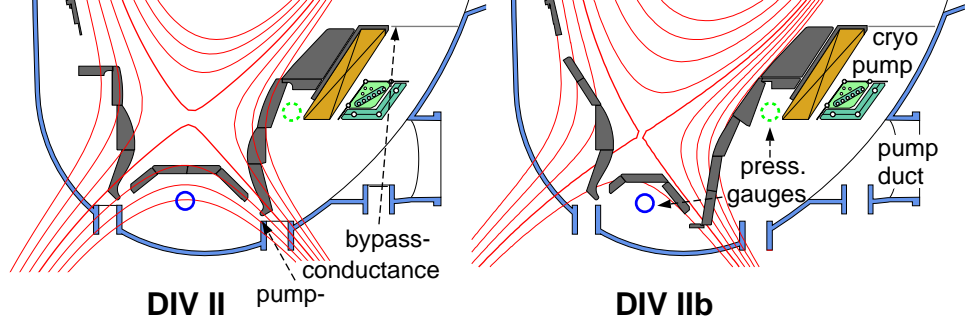


Figure 1. DIV II and the new DIV IIb with low and high δ plasma equilibria. The pressure gauges in the divertor below the roof baffle (solid circle) and in the pumping chamber (dashed circle), which were used to derive the bypass conductances in Sec.4 were also shown.

More details on the design of DIV IIb can be found in [7]. The conductance to the cryo-pump is not affected and due to the simpler shape of the outer strike point module, the diagnostic access is substantially facilitated. All diagnostics available already in DIV II (see [8] and references therein), were adapted accordingly. Operation with the new DIV IIb has been resumed successfully in April 2001 and more than 300 successful plasma discharges with different shaping and heating powers up to 13 MW have been performed till the end of the campaign at the end of July 2001.

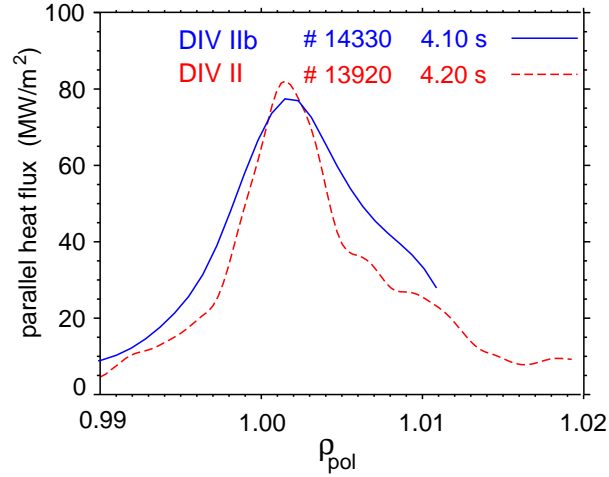


Figure 2. Parallel heat flux at the outer strike point in DIV IIb (#14330, $\bar{n}_e \approx 6.6 \cdot 10^{19} \text{m}^{-3}$, solid line) and DIV II (#13920, $\bar{n}_e \approx 5.1 \cdot 10^{19} \text{m}^{-3}$, dashed line) during a 5MW NBI-heated H-Mode discharge.

3. Power Deposition and Divertor Radiation

Experiments in the DIV II configuration suggested that the "inward" reflection of neutrals at the vertical target was a key point for the reduction of the parallel heat flux by a factor of two [8]. Even shifting the strike points upwards by nearly 10 cm away from the V-shaped, narrow divertor corners to a region above the roof baffle had little effect on the heat flux profiles. In DIV IIb the outer strike-point of the low triangularity equilibrium (which was the standard shape in DIV II) lies also clearly above the baffle region. Due to the larger angle between the strike point

module and the flux surfaces in the poloidal plane, a higher peak power density but a smaller profiles width along the target is expected. Indeed the thermographic measurements show that the maximum heat flux perpendicular to the target is higher by 50% compared to DIV II for otherwise comparable low density H-Mode discharges. Indeed, when taking into account the pitch angle it a nearly identical parallel heat flux can be extracted (see Fig. 2). A slightly broader (projected) profile is obtained for DIV IIb, leading to an integrated power load which is moderately increased compared to DIV II. According to spectroscopic measurements and modeling, the reduction of the power load in DIV II was attributed to strong carbon radiation in the dense divertor plasma [8]. This resulted also in a substantial increase of the total divertor radiation (compared to DIV I) to values of about 40% almost independent from the total heating power [9]. Figure 3 shows the fraction of the divertor radiation in DIV IIb, i.e. the radiation below a virtual horizontal line through the X-point. For comparison the values for DIV I and DIV II are included also. Comparing DIV IIb and DIV II for low δ , similar radiation levels are found, although in DIV IIb the strike points

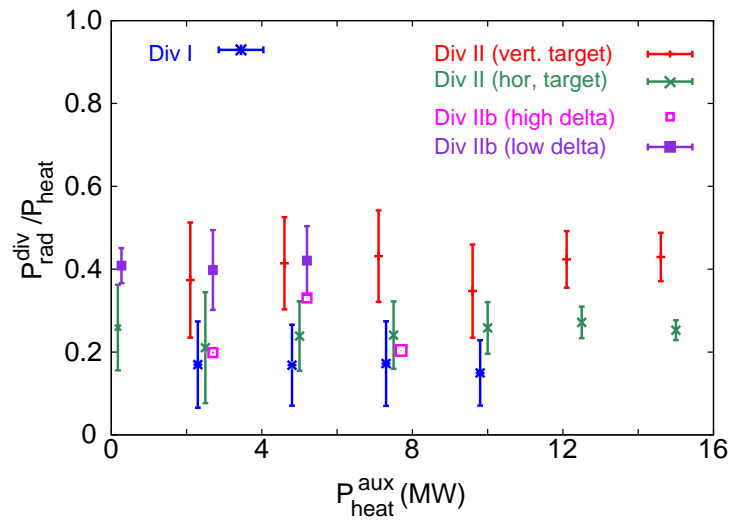


Figure 3. Fraction of the divertor radiation over the total heating power for different divertors and configurations. The vertical bars indicate the range due to additional parameter variation, especially operation at different densities.

are well above the baffled region, confirming the results from the z-shift in DIV II. For medium to high triangularity discharges the outer divertor leg is now placed on the vertical target instead on the roof baffle (horizontal) target. For these kind of discharges, the volume below the x-point is smaller by about 30%, explaining for about half of the lower radiation. Since the radiation levels are similar in this case in DIV II and DIV IIb, the lower values have to be attributed to more subtle effects like effective divertor depth and different power flows in the separatrix than just the change in the target orientation. This hypothesis is supported by detailed radiation profile measurements performing sweeps of the divertor fans to increase the spatial resolution of the bolometer system. These show very different radiation patterns for similar parameters of the main plasma. In the case of low triangularity discharges a rather symmetric in-out radiation pattern is found (as also presented for DIV II in [9]), whereas for higher δ 's the radiation is concentrated to the region between the x-point and the inner strikepoint.

4. Divertor Plasma-Parameters and Pumping Characteristics

Experiences in ASDEX Upgrade and JET [1] show that the geometry of the divertor can strongly influence the plasma parameters in the divertor and to certain degree also in the main chamber plasma edge. This may diminish the operation window in terms of the formation of MARFES, but early onset of detachment leads also to the desired strong reduction of the power flowing to the divertor plates [10, 11]. The divertor plasma parameters are measured by a set of Langmuir probes and complete profiles are again achieved by sweeping the divertor fans. The ELM

averaged maximum electron temperature at the separatrix at the outer target in DIV IIb is higher by 10 eV ($\approx 50\%$) than in DIV II during similar low density H-Mode discharges ($\bar{n}_e \approx 6 \cdot 10^{19} \text{ m}^{-3}$, 2.5MW NBI-heated), whereas in the SOL, T_e is quite similar in both divertors.

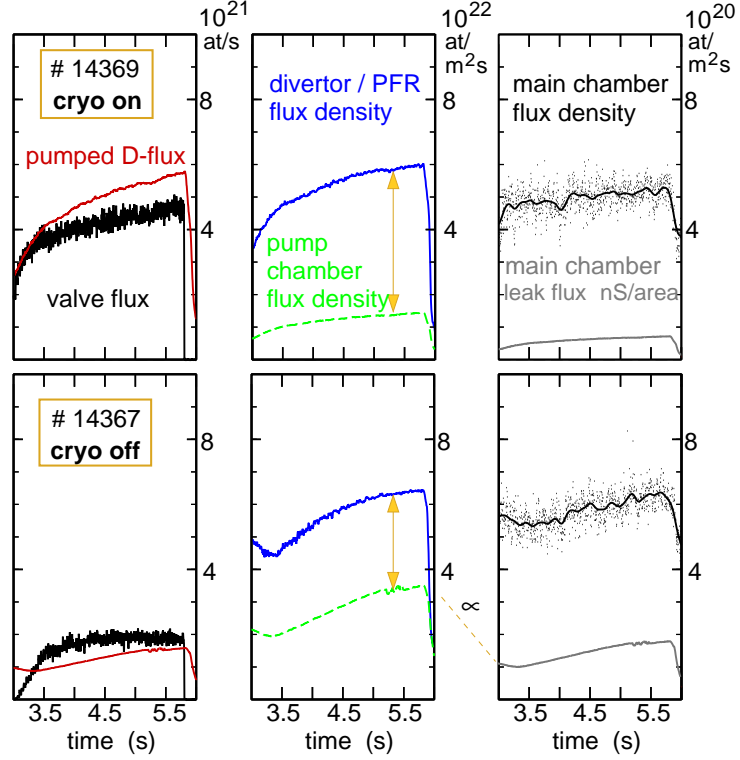


Figure 4. L-mode discharges ($I_p = 1$ MA, 1.4 MW NBI heating) with different pumping speeds (cryo-pump switched on (#14369) and off (#14367)) demonstrate the effect of pumping and bypass conductances on the main chamber and the pump chamber neutral pressure.

The neutral flux densities are measured by ionisation gauges at different locations in the vacuum vessel. Of special interest for the investigation presented here, are the fluxes below the roof baffle, in the pumping chamber (positions shown in Fig. 1) and above the outer midplane. First comparisons show that for the old standard configuration (low δ) as well as for higher triangularities no distinct differences in the neutral pressures are found, in contrast to simulations with the B2-Eirene code, which predicted a reduction of the pump duct flux densities by up to one order of magnitude [12] for similar discharges. This might be explained by the fact that the divertor neutral pressure is mainly maintained by the colder inner divertor leg, the configuration of which remained unchanged, and that the plugging by the outer leg is still effective despite its large distance to the gap.

To investigate the influence of the divertor bypasses on the effective exhaust rate in DIV IIb and on the main chamber recycling dedicated experiments were performed. The effective exhaust rate depends on the pumping speed of the turbo-molecular and cryo-pump as well as on the network of conductances between main chamber, divertor and pumping chamber. Of particular interest is the bypass conductance between pump chamber and main chamber (see Fig. 1), which reduces the effective pumping speed and may also lead to increased neutral fluxes in the main chamber. Fig 4 shows a comparison of 2 dedicated L-mode pulses with cryo-pump on and off used to determine the effect of the bypass conductance. The major effect of the stronger pumping is the reduction of pump chamber neutral pressure and a larger gas flow necessary to keep the feedback-controlled core plasma electron density. Using the known pumping speeds ($S_{cryo} = 110 \text{ m}^3/\text{s}$, $S_{turbo} = 14 \text{ m}^3/\text{s}$) of the pumps with respect to the pump chamber volume, the values of the two conductances can be derived from the particle balance equations for the pump volume for the two discharges. Wall pumping in the pump chamber is neglected, but this is assumed to be small

due to the fact that the neutrals are expected to be mostly low energy molecules here. Values of $S_{divertor-pump} = 70 \text{ m}^3/\text{s}$ and $S_{pump-main} = 40 \text{ m}^3/\text{s}$, are obtained by this procedure with an uncertainty of $\pm 10 \text{ m}^3/\text{s}$ each. Taking the value of the bypass conductance and the measured pump chamber neutral pressure, the neutral flux into the main chamber can be calculated. Divided by the plasma surface on the low field side (25 m^2), its contribution to the main chamber recycling is a factor of 3-5 below the measured value as shown in Fig. 4. This finding suggests the presence of radial ion fluxes to the wall causing the major part of the main chamber neutral recycling. These ion fluxes, and corresponding fluxes of light intrinsic impurities, may also be responsible for the observed characteristic of the tungsten sputtering at the main chamber walls [13, 14].

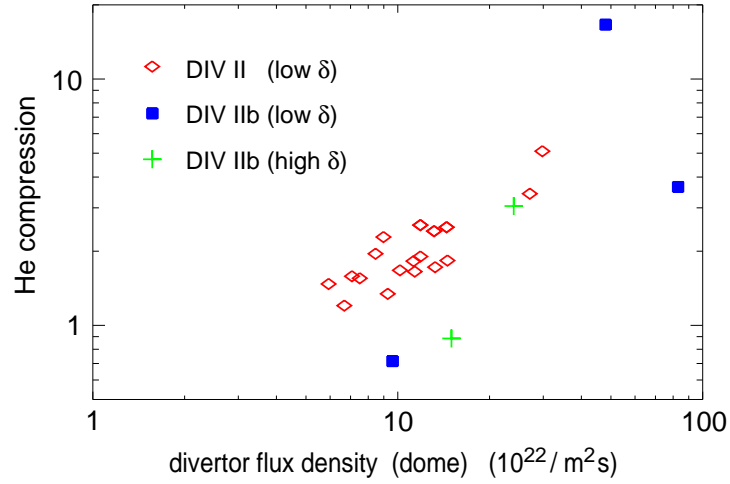


Figure 5. He compression in DIV II and DIV IIb for 5 MW NBI heated discharges as a function of the neutral flux density below the dome.

A key feature of DIV II was the high He compression ($C_{He} = n_{He,0}^{div} / n_{He,+}^{core}$) accomplished by the narrow divertor channel which hindered efficiently the back flow of neutral He [15]. This behaviour was reproduced by B2-Eirene model calculations, which predicted also a degradation of the compression accompanied by the strong decrease of the hydrogen flux density in the pumping plenum for comparable discharge conditions [12]. Following the procedure described in [15], the He compression in DIV IIb was evaluated from the He exhaust time constant via the three chamber model. The volumes below the dome and of the pumping chamber were adjusted in order to consider the slightly different geometry. The results support the trend predicted by the modeling, however the reduction is much smaller than expected from the calculations. Fig. 5 shows a comparison of the He compression in DIV II [15] and DIV IIb for 5 MW NBI heated discharges as a function of the neutral flux density below the dome. The data in DIV II (diamonds) were all taken at low triangularity, whereas the data of DIV IIb comprise low (squares) and high (crosses) triangularity discharges. Although there are too few measurements available for the DIV IIb to be conclusive, it seems that the dependence of C_{He} on the divertor flux density is more pronounced in DIV IIb. The decrease of the compression for highest flux densities is similar to findings in DIV II (at different heating powers). There it was explained by the re-opening of the divertor caused at the low electron temperatures, leading to mean free paths for neutral He large enough to escape the divertor.

5. Divertor Effect on the H-mode Threshold

In order to monitor the conditioning of the machine as well as to obtain a measure for the 'natural' scatter of threshold and confinement data a 'standard' H-Mode discharge is performed routinely since 1999 on a daily basis. These discharges are performed at $I_p = 1 \text{ MA}$, $B_t = 2 \text{ T}$, $q \approx 3.2$, $\delta \approx 0.3$. and the density is feedback controlled during the power ramp to $\bar{n}_e = 4.2 \cdot 10^{19} \text{ m}^{-3}$. Comparing the L-H transition power threshold for a clear reduction

by about 20% is found for DIV IIb compared to DIV II. Fig. 6 shows the evolution of the power threshold as a function of the number of discharges performed since the last major shut down. For both divertors there is a transient phase of conditioning observed for about 100 shots after the startup. However, as can be judged from the figure, the reduction is clearly found for all phases, and the scatter in the data, resulting mostly from the uncertainty in the applied heating power (the power ramp is done by chopping the NBI) is significantly smaller. More details about the long term behaviour of these 'standard' H-Mode discharges are presented elsewhere [16]. Lithium beam measurements in the midplane indicate that the density at the nominal separatrix and in the scrape-off layer is lower at the L-H transition, pointing out the importance of local edge parameters, as already seen after the change from DIV I to DIV II, where an increase of the threshold was found [1]. At the moment it is not clear whether these observations are due to the simultaneously installed tungsten coated central column (see [17, 18]) or whether they have to be attributed to the new divertor geometry.

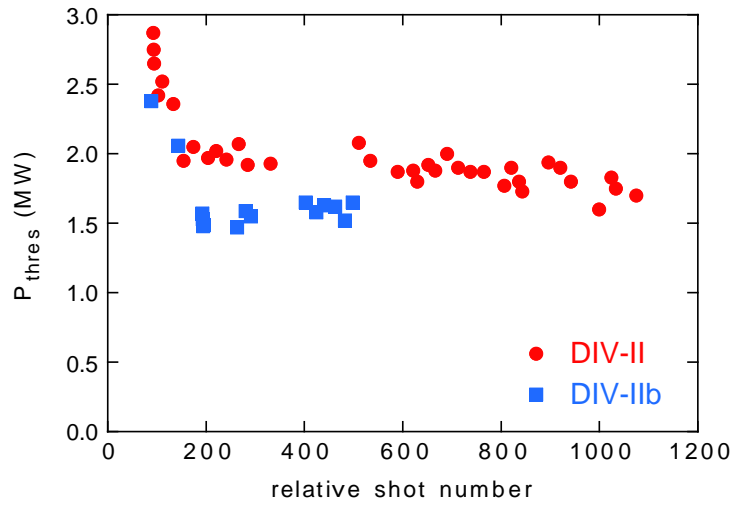


Figure 6. Evolution of H-Mode threshold for 'standard' H-Mode discharges in DIV II and DIV IIb

6. Summary and Outlook

The plasma operation was successfully started with the new DIV IIb and equilibria with $0.3 < \delta_{bot} < 0.5$ and additional heating powers up to 13MW were already used. The first characterization of DIV IIb revealed, that overall the beneficial properties of DIV II are essentially maintained. The transition from a well adapted case for one equilibrium (as it might be the case also in ITER), to a more flexible experimental solution, which can accommodate the full range of desired equilibria in ASDEX Upgrade, caused only minor changes to the divertor performance. The expected increase of the perpendicular power load and the increased electron temperatures at the outer strikepoint are still acceptable and the divertor radiation for similar magnetic configuration is almost unchanged. The decrease of the divertor radiation in high triangularity discharges obviously cannot exclusively be attributed to the operation with horizontal target plates, as it was concluded during DIV II operation, since it is very similar also for the vertical target operation of these discharges in the new DIV IIb configuration. The different radiation profiles for low and high δ point rather to more subtle effects, possible caused by different power flow patterns. In some contradiction to simulations with the B2-Eirene code, there is no strong reduction of the pump duct flux densities and the He compression for identical discharges in DIV II and DIV IIb. This may point to large influence of the inner divertor leg, the configuration of which remained unchanged. A significant reduction (20%) of the L-H threshold is observed which may be connected to lower separatrix/SOL densities upstream in the midplane as indicated by Li-beam measurements.

The reported behaviour will be examined in more detail in the forthcoming campaign. In addition to a detailed characterization of edge and divertor, an important question is to which extent the observed differences are caused by the simultaneous installation of large tungsten surfaces in the main chamber.

- [1] H.-S. Bosch, J. C. Fuchs, J. Gafert, G. Haas, A. Herrmann, A. Kallenbach, M. Kaufmann, J. Neuhauser, F. Ryter, R. Schneider, J. Schweinzer, W. Ullrich, U. Wenzel, G. C. Vlases, L. D. Horton, G. F. Matthews, ASDEX Upgrade Team, and JET Divertor Physics Topic Group, *Plasma Phys. Controlled Fusion* 41, A401 (1999).
- [2] A. Kallenbach, M. Kaufmann, D. P. Coster, J. C. Fuchs, A. Herrmann, J. Neuhauser, R. Schneider, K. Borrass, H.-S. Bosch, A. Carlson, J. Gafert, K. Lackner, K. Schmidtman, J. Schweinzer, W. Suttrop, U. Wenzel, and ASDEX Upgrade Team, *Nucl. Fusion* 39, 901 (1999).
- [3] G. Saibene et al., *Nucl. Fusion* 39, 1133 (1999).
- [4] J. Stober, O. Gruber, A. Kallenbach, V. Mertens, F. Ryter, A. Stähler, W. Suttrop, W. Treutterer, and ASDEX Upgrade Team, *Plasma Phys. Controlled Fusion* 42, A211 (2000).
- [5] T. Osborne et al., *Plasma Phys. Controlled Fusion* 42, A175 (2000).
- [6] J. Stober et al., *to be published in Plasma Phys. Control. Fusion* (2001).
- [7] O. Gruber et al., Combined Application to the HGF Strategy Fund for the Funding Period 1999 - 2002 from the HGF Centres, IPP Garching and FZ Jülich, for 'Optimized Stationary Tokamak Operation', Technical Report 1/322, IPP, Garching, Germany, 1999.
- [8] A. Kallenbach, D. Coster, J. C. Fuchs, H. Y. Guo, G. Haas, A. Herrmann, L. D. Horton, L. C. Ingesson, C. F. Maggi, G. F. Matthews, R. D. Monk, J. Neuhauser, F. Ryter, J. Schweinzer, J. Stober, W. Suttrop, ASDEX Upgrade Team, and J. Team, *Plasma Phys. Controlled Fusion* 41, B177 (1999).
- [9] J. Fuchs, D. Coster, A. Herrmann, A. Kallenbach, K. F. Mast, and ASDEX Upgrade Team, *J. Nucl. Mater.* 290–293, 525 (2001).
- [10] L. Horton et al., *Nucl. Fusion* 39, 1 (1999).
- [11] JET Team (prepared by R. Monk), *Nucl. Fusion* 39, 1751 (1999).
- [12] D. Coster, H.-S. Bosch, W. Ullrich, and ASDEX Upgrade Team, *J. Nucl. Mater.* 290–293, 845 (2001).
- [13] W. Schneider et al., Tungsten Migration between Main Chamber and Divertor of ASDEX Upgrade, in *Europhysics Conference Abstracts (Proc. of the 28th EPS Conference on Controlled Fusion and Plasma Physics, Funchal, 2001)*, 2001.
- [14] V. Rohde, R. Neu, K. Krieger, H. Maier, A. Geier, A. Tabasso, A. Kallenbach, R. Pugno, D. Bolshukhin, M. Zarrabian, and ASDEX Upgrade Team, Operation of ASDEX Upgrade with High-Z Wall Coatings, in *Plasma Physics and Controlled Nuclear Fusion Research ...*, volume 0, pp. –, Vienna, 2000, IAEA.
- [15] H.-S. Bosch, W. Ullrich, D. Coster, O. Gruber, G. Haas, J. Neuhauser, R. Schneider, R. Wolf, and ASDEX Upgrade Team, *J. Nucl. Mater.* 290–293, 836 (2001).
- [16] F. Ryter et al., Survey of H-Mode L-H Transition and Confinement from ASDEX Upgrade H-Mode Standard Shot, in *Proc. IAEA TCM on H-Mode Physics and Transport Barriers, Toki, Japan, 2001*, Vienna, 2001, IAEA.
- [17] V. Rohde et al., Tungsten as first wall material in the main chamber of ASDEX Upgrade, in *Europhysics Conference Abstracts (CD-ROM), Proc. of the 28th EPS Conference on Controlled Fusion and Plasma Physics, Funchal, 2001*, Geneva, 2001, EPS.
- [18] R. Neu et al., Impurity behaviour in the ASDEX Upgrade divertor tokamak with large area tungsten walls, in *Proc. IAEA TCM on Divertor Concepts, Aix en Provence, France, 2001*, Vienna, 2001, IAEA.